

¹ **Interannual variations of Atlantic tropical instability**
² **waves**

Renellys C. Perez^{1,2}, Rick Lumpkin², William E. Johns³, Gregory R. Foltz²,

Verena Hormann^{1,2}

¹Cooperative Institute for Marine and
Atmospheric Studies, University of Miami,
Miami, Florida, USA.

²NOAA Atlantic Oceanographic and
Meteorological Laboratory, Miami, Florida,
USA.

³Rosenstiel School of Marine and
Atmospheric Science, University of Miami,
Miami, Florida, USA.

Abstract. Observations are used to develop metrics for interannual tropical instability wave (TIW) variability in the Atlantic and to relate that variability to larger scale processes. The analysis is partitioned into different latitude bands to distinguish between off-equatorial (5°S , 2°N , and 5°N) and near-equatorial (2°S and 0°) TIWs. TIW metrics based on sea surface temperature (SST) and sea level anomaly (SLA) fluctuations are compared against interannual anomalies of SST in the cold tongue region. To examine the role of barotropic shear instabilities in modulating the intensity of a TIW season, wind stress and near-surface current indices are developed in regions where the shear between the Equatorial Undercurrent (EUC) and the northern branch of the South Equatorial Current (nSEC) and between the nSEC and the North Equatorial Countercurrent (NECC) are expected to be largest. Good agreement is found between the SST and SLA TIW metrics along the off-equatorial latitude bands, and interannual variations of both metrics can largely be attributed to barotropic shear instabilities. In particular, years with low (high) TIW variance along the off-equatorial latitude bands are associated with anomalously warm (cold) SSTs in the cold tongue region, weak (strong) wind stress divergence and curl in the EUC-nSEC region, and weak (strong) zonal current shear in the nSEC-NECC region. In contrast, in the near-equatorial latitude bands, poor agreement is found between interannual TIW activity based on the SST and SLA metrics, and near-equatorial TIW variability cannot be explained by the large-scale SST, wind stress divergence and curl, and current shear indices.

1. Introduction

The upper-ocean tropical Atlantic circulation is significantly modified by local winds and transient phenomena such as westward propagating tropical instability waves (TIWs) [Düing et al., 1975; Weisberg and Weingartner, 1988; Menkes et al., 2002; Foltz et al., 2004; Grodsky et al., 2005; Bunge et al., 2007; Dutrieux et al., 2008; von Schuckmann et al., 2008]. The local wind-forced circulation and TIW activity are connected through barotropic and baroclinic energy conversion and ocean-atmosphere interaction. Atlantic TIWs typically intensify in early boreal summer in response to the seasonal intensification of the southeasterly trade winds and the enhancement of meridional and vertical shear in the equatorial current system, and in phase with the onset of the equatorial Atlantic cold tongue [e.g., Grodsky et al., 2005]. In turn, it has been shown that once generated, the Atlantic TIWs can affect winds on short time and space scales through air-sea coupling [e.g., Caltabiano et al., 2005; Seo et al., 2007; Wu and Bowman, 2007a] and can reduce the shear of the background currents [e.g., Weisberg and Weingartner, 1988].

The intensity of an Atlantic TIW season can vary dramatically from one year to the next [e.g., Caltabiano et al., 2005; Wu and Bowman, 2007b, hereafter WB07; Athie and Marin, 2008, hereafter AM08], and dynamic downscaling experiments using an Intergovernmental Panel on Climate Change (IPCC) class model suggest that Atlantic TIWs are energized under global warming scenarios [Seo et al., 2011]. TIWs act to warm the near-surface and underlying waters of the equatorial Atlantic cold tongue on seasonal [e.g., Weisberg and Weingartner, 1988; Foltz et al., 2003; Jochum et al., 2004; Peter et al., 2006] and climate relevant time scales [Seo et al., 2011]. The mechanisms modulating TIW intensity and

fluxes in the equatorial Atlantic are therefore of great interest, because they could act to modulate the interannual intensity of the cold tongue.

Two distinct types of TIWs exist in the Atlantic: mixed Rossby-gravity (Yanai) waves near the equator with periods of 14 to 40 days, and Rossby waves between 2° to 5° latitude with periods of 20 to 50 days [e.g., Bunge et al., 2007; AM08; Han et al., 2008; von Schuckmann et al., 2008]. There is a general consensus that barotropic instabilities associated with the near-surface (upper 50 m) meridional shear between the northern branch of the westward flowing South Equatorial Current (nSEC) and the eastward flowing North Equatorial Countercurrent (NECC) are important for generating and sustaining Atlantic TIWs [e.g., Philander, 1978; von Schuckmann et al., 2008]. Barotropic or baroclinic shear instabilities associated with near-surface meridional or vertical shear between the eastward flowing Equatorial Undercurrent (EUC) and the nSEC may also play an important role [e.g., Weisberg and Weingartner, 1988; Grodsky et al., 2005; von Schuckmann et al., 2008]. However, the full suite of TIW generation processes and the range of latitudes in which they act are not well understood.

TIWs were first detected with satellite SST imagery in the Pacific Ocean by Legeckis [1977] and in the Atlantic Ocean by Legeckis and Reverdin [1987]. Subsequently, TIW signatures were found in sea level anomaly (SLA) fields measured by altimeters, with SST crests (troughs) associated with SLA lows (highs) [e.g., Malardé et al., 1987; Musman, 1989; 1992], as well as in 10-m wind stress estimated from scatterometers [e.g., Xie et al., 1998; Chelton et al., 2001]. Recently, WB07 demonstrated from eight years (1998 to 2005) of SST measurements from the Tropical Rainfall Measuring Mission (TRMM) Microwave Imager (TMI) that there is a strong negative correlation between TIW related

SST variance and area-averaged tropical Atlantic SST anomalies in the region bounded by 20°W and 0° and 3°S and 3°N (ATL3 index) in boreal summer. That is, TIW SST variance tends to be largest when the equatorial cold tongue is strongest. However, as noted in WB07, TIWs can best be observed using SSTs when the meridional gradients of SST across the cold tongue are large (e.g., during the cold phases of the ATL3 index as well as the seasonal peak of the cold tongue), and TIW variability may be underestimated in the SST record when meridional gradients are small (e.g., during the warm phases of the ATL3 index as well as the onset and decay phases of the cold tongue). Moreover, in WB07, TIW SST variance was computed in the region bounded by 35°W and 0° and 0° and 5°N . This treatment convolves the different types of Atlantic TIWs, that have different latitudes of maximum amplitude, into one broadband process. Using the same time period as the WB07 study, AM08 demonstrated that altimetric SLA fields could be used as a measure of TIW season intensity that is independent of the strength of the meridional SST gradient. Therefore, an analysis of TIWs using metrics based on SST and SLA partitioned into different latitude bands should help to quantify the interannual variability associated with near-equatorial TIWs and off-equatorial TIWs, and set the stage for examining their possible linkages to larger scale processes.

In this paper, the robustness of the relationship between the ATL3 index and interannual TIW variability is examined for the period 1998 to 2010 (i.e., the thirteen completed years of TMI measurements). In particular, we test the consistency of this relationship in terms of both TIW-related SST and SLA variance in order to more robustly establish the linkage between cold tongue intensity and TIW activity. The calculations are partitioned into five latitude bands to distinguish between the interannual variability of the different

types of Atlantic TIWs. In addition, we quantify the relationship between the SST and SLA TIW metrics for the five latitude bands, and extend the SLA TIW variance time series to encompass the full eighteen-year altimetric record. To examine the role of near-surface barotropic shear instabilities in modulating the intensity of a TIW season, wind stress and near-surface current indices are developed and compared against the TIW variability and the ATL3 index. These new indices provide information about the strength of the meridional gradient of the zonal currents ($\frac{\partial \bar{u}}{\partial y}$), an important component of the barotropic conversion term ($-\rho \overline{u'v'} \frac{\partial \bar{u}}{\partial y}$) in the TIW energy balance equation [e.g., Weisberg and Weingartner, 1988; Grodsky et al., 2005; von Schuckmann et al., 2008].

2. Data and methodology

2.1. Data

Four gridded data products are used in this analysis: TMI SST distributed by Remote Sensing Systems, altimetric delayed-time reference SLA fields distributed by AVISO, wind stress divergence and curl fields calculated on a swath-by-swath basis from Quick Scatterometer (QuikSCAT) wind measurements [Risien and Chelton, 2008], and near-surface currents derived from a synthesis of drifter velocities, altimetry and wind products [Niiler et al., 2003; Lumpkin and Garzoli, 2011 and references therein]. TMI SST daily (3-day running average) and monthly fields are available from January 1998 to present on a 0.25° spatial grid. AVISO reference SLA are obtained as weekly averages from October 14, 1992 to December 1, 2010 with $1/3^\circ$ spatial resolution, and are linearly interpolated to daily intervals. The reference SLA product pairs data from an altimeter with a 10-day repeat cycle and 315 km zonal spacing at the equator between successive ground tracks (Topex/Poseidon, Jason-1, or Jason-2) with data from an altimeter with a 35-day repeat

cycle and 80 km equatorial spacing between ground tracks (ERS-1, ERS-2, and Envisat), and can resolve 100-to-300 km scales which is adequate for capturing the variability associated with the $O(1000 \text{ km})$ zonal wavelength of TIWs [e.g., Legeckis, 1977; Qiao and Weisberg, 1995, and references therein]. Finer spatial resolution could be achieved by using the AVISO up-to-date SLA product, which merges data from up to four altimeters, but the sampling of that time series is not as stable as the reference product. Monthly QuikSCAT wind stress divergence and curl are available from September 1999 to October 2009 on a 0.25° grid. Poleward of 2.5° latitude, the drifter-altimetry synthesis produces weekly snapshots of Ekman and total (Ekman plus geostrophic) currents at 15-m depth that are derived from the AVISO SLA fields, with spatially-varying gain coefficients and time-mean field calculated to minimize the mean squared difference between geostrophic current anomalies and concurrent Ekman-removed drifter velocities [Niiler et al., 2003].

In situ horizontal velocity data from the 10-m current meter on the Prediction and Research Moored Array in the tropical Atlantic (PIRATA) Northeast Extension mooring at 4°N , 23°W from June 11, 2006 to July 25, 2010 [Bourlès et al., 2008] are used for comparison with the gridded data products. This data set provides a direct measurement of the interannual variations in kinetic energy associated with TIWs, and is related to TIW-related SST variability through the horizontal advection terms in the heat balance equation and to TIW-related SLA variability through geostrophy. Although horizontal velocity data is also available at the PIRATA 0°N , 23°W mooring, gaps in this record were sufficiently large from 2008 to 2010 that data from this site is not included in the analysis. Moreover, at the equator, other transient phenomena such as eastward propagating intraseasonal Kelvin waves are present with similar time scales of 40-to-60 days [e.g., Katz

1997; Han et al. 2008; Hormann and Brandt, 2009] that could influence estimates of TIW
variance based on a point measurement.

2.2. TIW variance

TIW-related SST and SLA variance are computed and compared for the overlap between
the TMI and AVISO records, 1998 to 2010. To isolate westward propagating TIW signals
and reduce variability associated with large-scale heating and cooling (e.g., steric effects),
a temporal and zonal band-pass Bartlett (i.e., triangle) filter is applied to the daily SST
and SLA data. This filter has a 20-to-50 day temporal and 4°-to-12° zonal window, and
has better side-lobe properties than the boxcar filter applied to SST in WB07. Hanning
and frequency-domain filters were also tested and produced similar results as the Bartlett
filter (not shown). Because a zonal band-pass filter cannot be applied to the time series of
horizontal velocity at the 4°N, 23°W mooring, this data set is only band-pass filtered in
time (20-to-50 day). Note, the cutoffs for the temporal band-pass filter were selected based
on spectral analysis of TMI SST and AVISO SLA in the equatorial Atlantic previously
conducted by AM08.

WB07 averaged Atlantic TIW activity from June to August and did not take into
account interannual variations in the month of peak TIW variability [Caltabiano et al.,
2005; AM08]. Here, TIW-related variance is computed over a 4-month sliding window
to allow the month of peak TIW activity to change from year to year. Variance is then
box-averaged in five 2° wide latitude bands centered on 5°S, 2°S, 0°, 2°N, and 5°N from
25°W to 0° (Figure 1a,b). Note that the 5°N band is terminated at 10°W due to the
basin geometry. This partitioning of variance with latitude allows for characterization
of interannual variability of near-equatorial and off-equatorial TIWs. At the 4°N, 23°W

mooring, the 4-month sliding window variance is only computed when a minimum of 15 daily records is available.

2.3. Indices

2.3.1. ATL3 index

The ATL3 index as first defined by Zebiak [1993] is the Atlantic counterpart to the Pacific Niño3.4 index, and is computed in the following manner from the monthly TMI SST data set. At each grid point in the ATL3 region (Figure 1c), seasonal cycles are generated by fitting SST to an annual and semi-annual cycle for the overlapping time period between TMI SST, QuikSCAT wind stress, and drifter-altimetry synthesis data (September 1999 to October 2009). The seasonal cycles are removed to generate monthly SST anomalies for the thirteen-year TMI record (1998 to 2010). These monthly anomalies are then averaged over the ATL3 region.

2.3.2. Barotropic shear indices

Indices are developed for the strength of the meridional gradient of the near-surface zonal currents in the northern half of the ATL3 region (20°W and 0° and 0° and 3°N) and just north of the ATL3 region (20°W and 0° and 3°N and 6°N) where the negative shear associated with the EUC-nSEC and the positive shear associated with the nSEC-NECC are expected to be large, respectively (Figure 1c). Although meridional shear between the EUC-nSEC is largest beneath the surface mixed layer (e.g., Figure 2 in Brandt et al. [2010]), the meridional shear between the EUC-nSEC has a strong near-surface expression that can generate and sustain TIWs.

The 15-m drifter-altimetry synthesis is calculated poleward of 2.5° latitude, and direct measurements of the meridional gradients of the total (Ekman plus geostrophic) zonal

currents can be obtained in the nSEC-NECC region. Meridional gradients are computed using centered differences at each grid point in the nSEC-NECC region, the seasonal cycles are removed, and the total zonal current shear anomalies are then box-averaged.

In absence of direct current measurements near the equator from which to estimate meridional shear in the EUC-nSEC region (Figure 1c), wind stress divergence and curl indices are computed from the monthly QuikSCAT data set. Wind stress divergence and curl are developed as indices because close to the equator they provide information about the strength of wind-driven vertical motion and the strength of the meridional gradient of the wind-driven zonal currents, respectively [e.g., Cane, 1979; Lagerloef et al., 1999; Wittenberg, 2002; Okumura and Xie, 2004; Perez and Kessler, 2009]. This can be seen from the simple equatorially-modified Ekman model applied in Perez and Kessler [2009], where wind-driven zonal and meridional transport, U_τ and V_τ , are given by

$$(U_\tau, V_\tau) = \left(\frac{r_s \tau_x + f \tau_y}{\rho_0(f^2 + r_s^2)}, \frac{r_s \tau_y - f \tau_x}{\rho_0(f^2 + r_s^2)} \right) \quad (1)$$

where τ_x and τ_y are the zonal and meridional components of wind stress, ρ_0 is seawater density, $f = 2\Omega \sin \theta$ ($\Omega = 7.29 \times 10^{-5} \text{ s}^{-1}$, θ is the latitude) is the Coriolis parameter, and r_s is the vertical shear dissipation rate. The wind-driven vertical velocity is given by the divergence of (U_τ, V_τ) and has the form

$$w_\tau = \frac{r_s \text{div}(\tau_x, \tau_y) + f \text{curl}(\tau_x, \tau_y)}{\rho_0(f^2 + r_s^2)} + \frac{\beta(f^2 - r_s^2)\tau_x - 2f\beta r_s \tau_y}{\rho_0(f^2 + r_s^2)^2} \quad (2)$$

where $\beta = \partial f / \partial y = 2.28 \times 10^{-11} \text{ m}^{-1} \text{ s}^{-1}$. From (1) the meridional shear of wind-driven zonal transport is given by

$$\frac{\partial U_\tau}{\partial y} = \frac{r_s \frac{\partial \tau_x}{\partial y} + f \frac{\partial \tau_y}{\partial y}}{\rho_0(f^2 + r_s^2)} - \frac{\beta(f^2 - r_s^2)\tau_y + 2f\beta r_s \tau_x}{\rho_0(f^2 + r_s^2)^2} \quad (3)$$

in that region. In this formulation, it is assumed that r_s is constant and spatial and temporal variations of the surface mixed layer thickness have been neglected. Moreover, remote influences from zonal winds in the western Atlantic through equatorial Kelvin waves are not represented in these equations [e.g., Servain et al., 1982]. Given these limitations, the following equations are merely provided to aid in the interpretation of the wind stress divergence and curl indices.

In the EUC-nSEC region, where f is assumed comparable in magnitude to r_s (e.g., $r_s^{-1} = 1.5 \text{ day} \approx f$ at 3°N), the first, third and fourth terms in equations (2) and (3) are all important for setting the strength of the mean wind-driven vertical velocity and the meridional shear of the wind-driven zonal transport. However, when limited to interannual variability, the first term in equations (2) and (3) carries over 75% percent of total variance (compare red and black lines in Figure 2), and for interannual anomalies (2) and (3) can therefore be approximated as

$$w_\tau \approx \frac{r_s \text{div}(\tau_x, \tau_y)}{\rho_0(f^2 + r_s^2)}, \quad (4)$$

and

$$\frac{\partial U_\tau}{\partial y} \approx \frac{r_s \frac{\partial \tau_x}{\partial y}}{\rho_0(f^2 + r_s^2)}. \quad (5)$$

216

217 On the time and length scales considered here for the index calculation (i.e., longer than
 218 TIW scales), equatorial wind stress divergence and curl are largely controlled by the
 219 meridional gradient terms, $\partial \tau_y / \partial y$ and $-\partial \tau_x / \partial y$, respectively. Therefore, (5) can be
 220 rewritten in terms of wind stress curl

$$\frac{\partial U_\tau}{\partial y} \approx -\frac{r_s \text{curl}(\tau_x, \tau_y)}{\rho_0(f^2 + r_s^2)} \quad (6)$$

221

222 such that anomalous positive (negative) curl just north of the equator will increase (de-
 223 crease) the magnitude of the negative meridional shear between the EUC and the nSEC.
 224 Similarly, (4) shows that anomalous positive (negative) divergence will increase (decrease)
 225 equatorial upwelling in the EUC-nSEC region (red line in Figure 2). Equatorial upwelling
 226 sets the strength of meridional gradients of SST and dynamic height anomaly (Φ) across
 227 the cold tongue, and thereby controls the strength of the meridional shear of geostrophic
 228 zonal currents in the EUC-nSEC region. For example, the anomalous geostrophic current
 229 shear between the mean latitude of the nSEC core, θ (typically near 2°N), and the equator
 230 can be defined as

$$\left. \frac{\partial u_g}{\partial y} \right|_{\theta/2} = -\frac{g}{\theta} \left(\left. \frac{1}{f_\theta} \frac{\partial \Phi}{\partial y} \right|_\theta - \left. \frac{1}{\beta} \frac{\partial^2 \Phi}{\partial y^2} \right|_{0^\circ} \right), \quad (7)$$

231

232 where $\left. \frac{\partial u_g}{\partial y} \right|_{\theta/2}$ is negative if $\left. \frac{\partial \Phi}{\partial y} \right|_{\theta} > \frac{f_{\theta}}{\beta} \left. \frac{\partial^2 \Phi}{\partial y^2} \right|_{0^\circ}$. In other words, a large enough increase
 233 (decrease) in the strength of the meridional gradient of Φ with respect to $\left. \frac{\partial^2 \Phi}{\partial y^2} \right|_{0^\circ}$ can
 234 increase (decrease) the magnitude of the negative meridional shear between the EUC and
 235 the nSEC near the surface. This geostrophic current shear combined with the wind-driven
 236 zonal current shear inferred from (6) provides a mechanism for generating barotropic shear
 237 instabilities in the EUC-nSEC region. Although total (Ekman plus geostrophic) zonal
 238 current shear anomalies are calculated in the nSEC-NECC region, the Ekman component
 239 of the nSEC-NECC shear is also evaluated because it is most directly comparable to the
 240 wind-based indices used in the EUC-nSEC region.

3. Results

241 In this section, interannual TIW variability and its connection to larger scale processes
 242 in the tropical Atlantic are examined. We start by quantifying the relationship between
 243 the SST and SLA TIW variance for the different latitude bands, and then relate the TIW
 244 metrics to the five indices: SST anomalies averaged over the ATL3 region, wind stress
 245 divergence and curl anomalies averaged over the EUC-nSEC region, and 15-m Ekman and
 246 total zonal current shear in the nSEC-NECC region.

3.1. Interannual TIW variability

247 Figure 3 shows the normalized SST and SLA TIW variance (blue and black curves,
 248 respectively) as a function of time for the five latitude bands. For each latitude band
 249 and field, the variance time series is scaled by its maximum observed variance between
 250 the overlapping time period of 1998 to 2010 (see Table 1 for a list of these values). The

maximum SST TIW variance, $0.05\text{ }^{\circ}\text{C}^2$, is found along the 2°N latitude band during 2001, consistent with WB07 and AM08. Similarly, the maximum SLA TIW variance (1.04 cm^2) occurs in 2001 along the 5°N latitude band. Although consistent with AM08, in that they found 2001 to be a year of high SLA TIW variability, 2002 was the strongest TIW season in their analysis. Note that the maximum horizontal velocity TIW variance in the shorter PIRATA mooring record is $254.6\text{ cm}^2\text{s}^{-2}$ in 2009.

From Table 1 it is evident that SST TIW variance is large in the bands near the mean latitude of the northern cold tongue front (2°N and 0°), although significant variance is also found along the 5°N and southern (2°S and 5°S) latitude bands. In contrast, SLA TIW variance tends to be largest away from the equator along the 5°N and to a lesser extent the 5°S , 2°S , and 2°N latitude bands (Table 1) consistent with the cross-equatorial structure of shear-modified Rossby waves [e.g., Lyman et al., 2005; AM08].

The month of peak TIW activity changes from year to year. The two most likely months for the annual maximum in SST and SLA variance along the northern latitude bands (2°N and 5°N) are June and July (Table 2). In contrast, peak TIW variance is typically found in late boreal summer/early fall along the 0° and southern latitude bands. Hence, the seasonal peak in TIW variance is defined as the annual maximum between May and October to better represent TIW activity along the different latitude bands.

The seasonal peaks in SST and SLA TIW variance (black and blue stars in Figure 3a,b,e) are highly correlated with one another (correlations between 0.65 and 0.75) for the 5°S , 2°N , and 5°N latitude bands. Along the northern latitude bands, the extreme events tend to be similar for the SST and SLA TIW metrics (Figure 3a,b). For example, during 2006 to 2009 there are three consecutive years (2006 to 2008) of anomalously low TIW

intensity followed by a very strong TIW season in 2009. These events are also observed in the horizontal velocity TIW variance record at the PIRATA mooring (red curve in Figure 3a). The ordering of the more moderate events, however, can differ between the two TIW metrics and between the two northern latitude bands (e.g., 2002 is a moderate-to-strong year for SST and SLA TIW variance at 2°N and the SLA TIW variance at 5°N , but it is a relatively weak year for the SST TIW variance at 5°N). The extent to which SST TIW variance along the 2°N and 5°N latitude bands depends on interannual variations in the strength of meridional SST gradients across the northern front of the cold tongue (i.e., the ATL3 index) vs. TIW dynamics will be explored in section 3.3.

Partitioning the variance by latitude shows that while TIW variance at 2°N and 5°N is modestly correlated with TIW variance along the 5°S latitude band, there is poor or negative correlation with TIW variance along the 2°S and 0° latitude bands (Table 3). The lack of correlation between the off-equatorial TIWs (defined here as the 5°S , 2°N , and 5°N latitude bands) and near-equatorial TIWs (2°S and 0°N latitude bands) helps to explain some differences between the ordering of TIW seasons in this study and previous studies. In WB07 and AM08, off-equatorial TIWs were convolved with near-equatorial TIWs in their measures of TIW season intensity. For instance, WB07 found 2004 to be a strong year based on their analysis of SST TIW variance from 0° to 5°N , while in the present analysis 2004 is the year of maximum SST TIW variance only along the 0° latitude band (Table 3).

The use of AVISO SLA allows the TIW variance time series to be extended back to the beginning of the altimetry record in late 1992 (Figure 3). Based on the longer record, off-equatorial TIWs appear to have been less energetic in the 1990s than in the 2000s.

In particular, there was another three year period of anomalously weak TIWs from 1997 to 1999 along the 5°N and 5°S latitude bands. In contrast, near-equatorial TIW activity was relatively low in the 2000s compared with the 1990s, with maximum TIW variance occurring during 1998.

3.2. Relationship of ATL3 SST with barotropic shear indices

The Atlantic zonal mode, represented by the ATL3 index, is the strongest source of interannual SST variability in the equatorial Atlantic. In this section, we therefore explore the relationship between the barotropic shear indices and the ATL3 SST index (Figures 4 and 5) before examining the connections between these indices and TIW intensity in the next section. A comparison of the ATL3 SST and wind stress divergence and curl indices (Figure 4a-c) shows that time periods (particularly during boreal summer) when SSTs in the tropical Atlantic cold tongue are anomalously warm (positive ATL3) such as the years 2006 to 2008, divergence and curl are anomalously weak (negative divergence and curl indices) in the EUC-nSEC shear region. Conversely, during time periods when the cold tongue is anomalously cold such as the years 2000 and 2001, divergence and curl are anomalously strong in the EUC-nSEC shear region. The correlation of ATL3 SST and wind stress divergence is particularly strong, and in fact ATL3 SST is more strongly correlated with divergence than it is with the zonal or meridional components of the wind stress in the central equatorial Atlantic. Note, Zebiak [1993] previously showed that zonal (meridional) pseudostress anomalies in the central tropical Atlantic were only modestly (poorly) correlated with the ATL3 index, but also found zonal pseudostress anomalies in the western equatorial Atlantic to be important in agreement with earlier studies [e.g., Servain et al., 1982].

Figure 4d demonstrates that there is nearly equivalent negative correlation between the ATL3 and divergence index at zero-lag and one-month lag ($r = -0.75$, SST slightly lags divergence) and negative correlation between the ATL3 and curl index at one-month lag ($r = -0.42$, SST lags curl). The strong relationship between the ATL3 SST and wind stress divergence is to be expected because wind-driven vertical motions, which modify cold tongue SST and the meridional shear of geostrophic zonal currents, depend on wind stress divergence near the equator (cf. section 2.3.2). Moreover, the ocean and atmosphere are coupled, and wind stress divergence and curl anomalies may be enhanced by SST anomalies via the Lindzen and Nigam [1987] mechanism [e.g., Okumura and Xie, 2004] and positive Bjerknes feedback [e.g., Keenlyside and Latif, 2007].

A similar comparison of the ATL3 SST index with the 15-m Ekman and total zonal current shear indices (Figure 5a-c) shows that periods with anomalously warm SST in the cold tongue region tend to be associated with weak Ekman and total zonal current shear in the nSEC-NECC shear region, and vice versa. While these relationships are not as strong as for wind stress divergence (compare Figures 4d and 5d), the correlations between the ATL3 index and Ekman zonal current shear ($r = -0.51$) and between the ATL3 and total zonal current shear ($r = -0.43$) are significant at one-month lag. Note that the total zonal current shear exceeds Ekman shear by almost an order of magnitude (different y-axis in Figure 5b,c), which means that geostrophic zonal current shear is important in the nSEC-NECC region.

3.3. Relationship of TIW intensity to SST and barotropic shear indices

To examine the larger scale processes that modulate TIW season intensity, the seasonal peaks in SST and SLA TIW variance (stars in Figure 3a,b) along the 2°N and 5°N latitude

bands are compared against the SST and barotropic shear indices. As the cold tongue and Atlantic TIWs typically intensify in early boreal summer, WB07 compared the SST TIW variance with the ATL3 index averaged from June to August. Here, the ATL3 averaging window is broadened from June to August to June to September, to account for years with delayed cold tongue onset. Wind stress divergence is also averaged from June to September, since it is nearly in phase with the ATL3 index (Figure 4d). The other indices are averaged from May to August, as they all lead the ATL3 index by one month (Figures 4d and 5d). Note, summer-time divergence and curl comparisons are limited to the years 2000 to 2009 due to the shorter QuikSCAT record length, whereas the other comparisons are made for the years 1998 to 2010. While the full-record correlations between the ATL3 index and the barotropic shear indices discussed in section 3.2 can be modest for some of the indices, the correlations between the summer-time averages of the indices are high, with values of -0.67 (ATL3-wind stress divergence), -0.71 (ATL3-wind stress curl), -0.92 (ATL3-Ekman zonal current shear), and -0.66 (ATL3-total zonal current shear). These correlations are all significant at the 95% confidence level.

Despite partitioning the SST TIW variance into latitude bands and adding five more years to the SST record, the WB07 ATL3-SST TIW variance relationship still holds (Figures 6a and 7a), with strong negative correlations between the ATL3 index and SST TIW variance of -0.86 along the 2°N latitude band and -0.74 along the 5°N latitude band. In particular, the anomalously warm summer SSTs during the years 2006 to 2008 coincide with some of the weakest TIW seasons in the thirteen-year record, when TIW seasonal intensity is characterized by the SST metric. Both the wind stress divergence and curl indices in the EUC-nSEC region describe well the SST TIW variance during

2000 to 2009 along both latitude bands with positive correlations between 0.7 and 0.83 (Figures 6b,c and 7b,c). Years with low TIW activity tend to have negative divergence (i.e., downwelling favorable) and negative curl anomalies in boreal summer, and vice versa, consistent with the relationships between TIW activity and the ATL3 index and between the ATL3 index and the large-scale wind pattern. In general, there is less spread in the curl-SST TIW variance relationship than the divergence-SST TIW variance relationship and better agreement with the wind-based indices along 5°N than along 2°N . SST TIW variance correlates quite strongly with the Ekman and total zonal current shear in the nSEC-NECC region for both latitude bands (Figures 6d,e and 7d,e) such that years of weak (strong) shear are typically associated with years of low (high) TIW activity.

When TIW season intensity is characterized by SLA variations rather than SST variations, those variations depend more on anomalous wind stress divergence and curl in the EUC-nSEC or anomalous current shear in the nSEC-NECC regions than on anomalous cold tongue SSTs (Figures 8 and 9). There are far more outliers in the relationship between SLA TIW variance along the 2°N and 5°N latitude bands and the ATL3 index (Figures 8a and 9a), and correlations are only significant along 2°N (-0.58). Although there is a great deal of spread in the wind stress divergence-SLA TIW variance relationship along the 2°N latitude band (Figure 8b), the curl-SLA TIW variance relationship is robust with a positive correlation of 0.71 (Figure 8c). Along the 5°N latitude band (Figure 9b,c) where the SLA response is largest (Table 1), the correlations between divergence and SLA TIW variance and between curl and SLA TIW variance are both significant (0.63 and 0.69, respectively). Ekman zonal current shear in the nSEC-NECC region explains SLA TIW variance well for both latitude bands (Figures 8d and 9d), but the total nSEC-

NECC current shear can only explain SLA TIW variance along the 5°N latitude band (Figure 9e).

Figure 10 shows correlations between SST and SLA TIW variance with the five indices for all latitude bands. For the indices tested here, correlations with SST and SLA TIW variance are all poor or of opposing sign for the near-equatorial (0° and 2°S) latitude bands. Although correlations are modest and not significant at the 95% level along the 5°S latitude band, TIW season intensity tends to vary at that latitude in the same way that it does at the northern latitudes. This suggests that the interannual TIW-band variance at 5°N and 5°S is linked [consistent with previous findings by AM08], and that the instability, even if drawing its energy mainly from current shear north of the equator, manifests itself as a shear-modified equatorial Rossby wave (cf. section 3.1).

4. Discussion and conclusions

A previous study by WB07 demonstrated that there is a strong relationship between TIW SST variability and SST anomalies in the equatorial Atlantic cold tongue region, such that TIW SST variance tends to be largest when the equatorial cold tongue is strongest and meridional SST gradients across the cold tongue are most pronounced. However, their study did not take into consideration (1) that different types of TIWs exist in the Atlantic with different latitudes of maximum amplitude, and (2) that the correlation between SST variance and large-scale SST gradient can be artificially heightened due to the “visibility” of the cold tongue front (e.g., TIWs can best be observed using SSTs when the cold tongue SST gradients are large), motivating a TIW metric based on SLA.

To address these issues, the ability to characterize interannual TIW variability in the Atlantic using both TMI SST and AVISO SLA was explored in this paper. Moreover, the

analysis was partitioned into five 2° wide latitude bands (5°S , 2°S , 0° , 2°N , and 5°N) to distinguish between near-equatorial and off-equatorial TIWs. Along each latitude band, interannual TIW variability was related to larger-scale processes by comparing with the summer-time averages of five indices: SST anomalies averaged over the ATL3 region, wind stress divergence and curl anomalies averaged over the EUC-nSEC region, and 15-m Ekman and total zonal current shear in the nSEC-NECC region. The wind and current shear indices were developed because they provide information about the strength of the meridional gradient of the near-surface zonal currents, and allow for examination of the role of barotropic shear instabilities in modulating the intensity of a TIW season. It was shown that the five indices were strongly linked in boreal summer, with decreased (increased) wind stress divergence and curl in the EUC-nSEC region as well as decreased (increased) Ekman and total zonal current shear in the nSEC-NECC region coincident with or preceding warming (cooling) of SSTs in the ATL3 region by one month.

Interannual variations of SST and SLA TIW variance were well correlated with each other along the off-equatorial latitude bands (5°S , 2°N , and 5°N) and poorly correlated with each other along the near-equatorial latitude bands (2°S and 0°) suggesting “visibility” is a problem for the SST metric at those latitudes. During 1998 to 2010, the largest amplitude TIW variations were found along 2°N for SST and 5°N for SLA, consistent with the sea level signature of equatorial Rossby waves and the position of the northern cold tongue front. The relative ordering of more moderate events along the northern (2°N and 5°N) latitude bands differed between the two TIW metrics. However, extreme events such as the three anomalous years of low TIW intensity during 2006-2008 followed by a

very strong TIW season in 2009 were similar for both metrics, and agreed well with TIW variance computed from data at the 4°N, 23°W PIRATA mooring.

AM08 demonstrated that interannual SLA TIW variations in the northern (0° to 8°N) and southern (8°S to 0°) hemispheres were related, however, their analysis convolved the different types of TIWs (see their Figure 9). By partitioning the variance into latitude bands, the present analysis expanded upon that result and showed that TIW variance north of the equator was modestly correlated with TIW variance along the 5°S latitude band, and poorly or negatively correlated with TIW variance along the near-equatorial latitude bands.

Along the northern latitude bands, the ATL3-SST TIW variance relationship was found to be robust, qualitatively consistent with WB07, and the anomalously warm summer SSTs during the years 2006 to 2008 coincide with some of the weakest TIWs in the thirteen-year SST record. In this study, however, it was further demonstrated that years with low (high) SST TIW variance along the northern latitude bands were typically associated with anomalously weak (strong) summer-time wind stress divergence and curl in the EUC-nSEC region as well as weak (strong) Ekman and total zonal current shear in the nSEC-NECC region. While all indices were strongly related to SST TIW variance, significant correlations with the SLA TIW variance were only found for the ATL3 SST, wind stress curl in the EUC-nSEC region, and Ekman shear in the nSEC-NECC region along the 2°N latitude band as well as for all of the wind and current shear indices along the 5°N latitude band. Although the correlations were modest and not significant at the 95% level for the 5°S latitude band, SST and SLA TIW variance tended here to be correlated with the five indices in the same way as the northern latitude bands suggesting that

the off-equatorial TIWs are governed by similar mechanisms. It is evident from the low or negative correlations between TIW variance along the near-equatorial latitude bands and the five indices tested here, that near-equatorial TIW variability cannot be explained by the large-scale SST, wind stress curl and divergence, and zonal current shear indices.

Interannual variations in the strength of the northern cold tongue front can influence the ordering of TIW seasons in the TIW metric based on SST relative to the metric based on SLA (i.e., there is some artificial heightening of SST TIW variability due to “visibility”). However, the correlation analyses conducted here indicate that the interannual variations of both SST and SLA TIW variance along the off-equatorial latitude bands can largely be attributed to barotropic shear instabilities between the nSEC and NECC. The data were insufficient to fully evaluate the dependence of interannual TIW variability on meridional shear between the EUC and nSEC, but the skill of wind stress divergence and curl in explaining TIW season intensity indicates that barotropic shear instabilities between the EUC and nSEC also play a role.

A previous model study by von Schuckmann et al. [2008] found baroclinic energy production in the nSEC-NECC region to be weaker than barotropic energy production in boreal summer (i.e., during the seasonal peak in TIW variance for the northern latitude bands, see Table 2). The role of baroclinic shear instabilities in driving interannual TIW variability was not examined in this study. However, high positive correlations (greater than 0.6) were found between the TIW metrics along the off-equatorial latitude bands and meridional SST gradients in the EUC-nSEC region (very similar to the ATL3 index) and modest correlations (between 0.2 and 0.6) were found between the TIW metrics and SST gradients in the nSEC-NECC region (not shown), indicating that baroclinic shear

instabilities may also be important in these regions. In order to develop better indices for TIW season intensity, analyses of the full barotropic and baroclinic conversion terms (e.g., $-\overline{\rho u'v'} \frac{\partial \bar{u}}{\partial y}$ and $-g \overline{v' \rho'} \frac{\partial \bar{\rho}}{\partial y} / |\frac{\partial \bar{\rho}}{\partial z}|$) need to be performed. This analysis requires knowledge of the meridional and vertical gradients of the background zonal currents (\bar{u}) and density field ($\bar{\rho}$), as well as the eddy flux terms (e.g., $\overline{u'v'}$ and $\overline{v'\rho'}$), which calls for the use of high-resolution ocean models that can provide a consistent representation of the upper-ocean circulation and density field that simultaneously resolve TIWs and larger scale processes, and ultimately long-term ocean observations at sites including the PIRATA moorings. Analysis of SLA TIW variance over the full altimetric record (Figure 3) shows potential decadal variations in TIW season intensity along the different latitude bands. Further model and observation based studies are needed to determine how these long-term variations in TIW season intensity impact the cold tongue heat balance in the equatorial Atlantic.

490 **Acknowledgments.** We thank the three anonymous reviewers and Gustavo Goni,
491 David Enfield, and Sang-Ki Lee for comments that improved the manuscript. This work
492 was supported by the NOAA/Atlantic Oceanographic and Meteorological Laboratory and
493 the Cooperative Institute for Marine and Atmospheric Studies at the University of Miami.
494 Microwave OI SST data are produced by Remote Sensing Systems and sponsored by the
495 National Oceanographic Partnership Program (NOPP), the NASA Earth Science Phys-
496 ical Oceanography Program, and the NASA MEaSUREs DISCOVER Project; data are
497 available at www.remss.com. The altimeter products were produced by Ssalto/Duacs and
498 distributed by Aviso, with support from Cnes (<http://www.aviso.oceanobs.com/duacs/>).
499 The QuikSCAT wind stress divergence and curl fields were provided by Craig Risien
500 and Dudley Chelton. PIRATA data are distributed by the TAO Project Office of
501 NOAA/PMEL (<http://www.pmel.noaa.gov/pirata/>).

References

- 502 Athie, G., and F. Marin (2008), Cross-equatorial structure and temporal modulation of
 503 intraseasonal variability at the surface of the Tropical Atlantic ocean, *J. Geophys. Res.*,
 504 *113*, C08020, doi:10.1029/2007JC004332.
- 505 Bourlès, B., R. Lumpkin, M. J. McPhaden, F. Hernandez, P. Nobre, E. Campos, L. Yu,
 506 S. Planton, A. Busalacchi, A.D. Moura, J. Servain, and J. Trotte (2008), The PIRATA
 507 program: history, accomplishments, and future directions, *Bull. Amer. Meteor. Soc.*,
 508 *89*, 1111–1125, doi:10.1175/2008BAMS2462.1.
- 509 Brandt, P. V. Hormann, A. Körtzinger, M. Visbeck, G. Krahmann, L. Stramma,
 510 R. Lumpkin, and C. Schmid (2010), Changes in the ventilation of the oxygen
 511 minimum zone of the tropical North Atlantic, *J. Phys. Oceanogr.*, *40*, 1784–1801,
 512 doi:10.1175/2010JPO4301.1.
- 513 Bunge, L., C. Provost, and A. Kartavtseff (2007), Variability in horizontal current ve-
 514 locities in the central and eastern equatorial Atlantic in 2002, *J. Geophys. Res.*, *112*,
 515 C02014, doi:10.1029/2006JC003704.
- 516 Caltabiano, A. C. V., I. S. Robinson, and L. P. Pezzi (2005), Multi-year satellite ob-
 517 servations of instability waves in the tropical Atlantic Ocean, *Ocean Sci. Discuss.*, *2*,
 518 1–35.
- 519 Cane, M. A. (1979), The response of an equatorial ocean to simple windstress patterns:
 520 I. Model formulation and analytic results, *J. Mar. Res.*, *37*, 233–252.
- 521 Chelton, D. B., S. K. Esbensen, M. G. Schlax, N. Thum, M. H. Freilich, F. J. Wentz,
 522 C. L. Gentemann, M. J. McPhaden, and P. S. Schopf (2001), Observations of coupling
 523 between surface wind stress and sea surface temperature in the eastern tropical Pacific,

524 *J. Clim.*, *14*, 1479–1498.

525 Düing, W., P. Hisard, E. Katz, J. Meincke, L. Miller, K. V. Moroshkin, G. Philander,
526 A. A. Ribnikov, K. Voigt, and R. Weisberg (1975), Meanders and long waves in the
527 equatorial Atlantic, *Nature*, *257*, 280–284, doi:10.1038/257280a0.

528 Dutrieux, P., C. E. Menkes, J. Vialard, P. Flament, and B. Blanke (2008), Lagrangian
529 study of tropical instability vortices in the Atlantic, *J. Phys. Oceanogr.*, *38*, 400–417,
530 doi:10.1175/2007JPO3763.1.

531 Foltz, G. R., S. A. Grodsky, J. A. Carton, and M. J. McPhaden (2003), Seasonal mixed
532 layer heat budget of the tropical Atlantic Ocean, *J. Geophys. Res.*, *108*, C5, 3146,
533 doi:10.1029/2002JC001584.

534 Foltz, G. R., J. A. Carton, and E. P. Chassignet (2004), Tropical instability vortices in the
535 tropical Atlantic Ocean, *J. Geophys. Res.*, *109*, , C03029, doi:10.1029/2003JC001942.

536 Grodsky, S. A., J. A. Carton, C. Provost, J. Servain, J. A. Lorenzzetti, and M. J.
537 McPhaden (2005), Tropical instability waves at 0°N, 23°W in the Atlantic: A case
538 study using Pilot Research Moored Array in the Tropical Atlantic (PIRATA) mooring
539 data, *J. Geophys. Res.*, *110*, C08010, doi:10.1029/2005JC002941.

540 Han, W., P. J. Webster, J. Lin, W. T. Liu, R. Fu, D. Yuan, and A. Hu (2008), Dynamics
541 of intraseasonal sea level and thermocline variability in the equatorial Atlantic during
542 2002–2003, *J. Phys. Oceanogr.*, *38*, 945–967, doi:10.1175/2008JPO3854.1.

543 Hormann, V., and P. Brandt (2009), Upper equatorial Atlantic variability during 2002
544 and 2005 associated with equatorial Kelvin waves, *J. Geophys. Res.*, *114*, C03007, doi:
545 10.1029/2008JC005101.

- Jochum, M., P. Malanotte-Rizzoli, and A. J. Busalacchi (2004), Tropical instability waves in the Atlantic Ocean, *Ocean Modell.*, *7*, 145–163.
- Katz, E. J. (1997), Waves along the equator in the Atlantic, *J. Phys. Oceanogr.*, *27*, 2536–2544.
- Keenlyside, N. S., and M. Latif (2007), Understanding equatorial Atlantic interannual variability, *J. Climate*, *20*, 131–142.
- Lagerloef, G. S. E., G. T. Mitchum, R. B. Lukas, and P. P. Niiler (1999), Tropical Pacific near-surface currents estimated from altimeter, wind, and drifter data, *J. Geophys. Res.*, *104*, 23313–23326.
- Legeckis, R. (1977), Long waves in the eastern equatorial Pacific Ocean: A view from a geostationary satellite, *Science*, *197*, 1179–1181.
- Legeckis, R., and G. Reverdin (1987), Long waves in the equatorial Atlantic Ocean during 1983, *J. Geophys. Res.*, *92*, 2835–2842.
- Lindzen, R. S., and S. Nigam (1987), On the role of sea surface temperature gradients in forcing low-level winds and convergence in the tropics, *J. Atmos. Sciences*, *44*, 2418–2436.
- Lumpkin, R., and S. Garzoli (2011), Interannual to decadal changes in the western South Atlantic’s surface circulation, *J. Geophys. Res.*, *116*, C01014, doi:10.1029/2010JC006285.
- Lyman, J. M., D. B. Chelton, R. A. deSzoeko, and R. M. Samelson (2005), Tropical instability waves as a resonance between equatorial Rossby waves, *J. Phys. Oceanogr.*, *35*, 232–254.

- 568 Malardé, J.-P., P. deMey, C. Péri­gaud, and J.-F. Minster (1987), Observations of long
569 equatorial waves in the Pacific ocean by Seasat altimetry, *J. Phys. Oceanogr.*, *17*, 2273–
570 2279.
- 571 Menkes, C. E., S. C. Kennan, P. Flament, Y. Dandonneau, S. Masson, B. Biessy, E. Mar-
572 chal, G. Eldin, J. Grelet, Y. Montel, A. Morlière, A. Lebourges-Dhaussy, C. Moulin, G.
573 Champalbert, and A. Herbland (2002), A whirling ecosystem in the equatorial Atlantic,
574 *Geophys. Res. Lett.*, *29*, 1553, doi:10.1029/2001GL014576.
- 575 Musman, S., (1989), Sea height wave form in equatorial waves and its interpretation, *J.*
576 *Geophys. Res.*, *94*, 3303–3309.
- 577 Musman, S. (1992), Geosat altimeter observations of long waves in the equatorial Atlantic,
578 *J. Geophys. Res.*, *97*, 3573–3579.
- 579 Niiler, P. P., N. A. Maximenko, G. G. Panteleev, T. Yamagata, and D. B. Olson (2003),
580 Near-surface dynamical structure of the Kuroshio Extension, *J. Geophys. Res.*, *108*, C6,
581 3193, doi:10.1029/2002JC001461.
- 582 Okumura, Y., and S.-P. Xie (2004), Interaction of the Atlantic equatorial cold tongue and
583 the African monsoon, *J. Clim.*, *17*, 3589–3602.
- 584 Philander, S. G. H. (1978), Instabilities of zonal equatorial currents, 2, *J. Geophys. Res.*,
585 *83*, 3679–3682.
- 586 Perez, R. C., and W. S. Kessler (2009), The three-dimensional structure of trop-
587 ical cells in the central equatorial Pacific ocean, *J. Phys. Oceanogr.*, *39*, 27–49,
588 doi:10.1175/2008JPO4029.1.
- 589 Peter, A.-C., M. Le Hénaff, Y. du Penhoat, C. E. Menkes, F. Marin, J. Vialard, G. Cani-
590 uax, and A. Lazar (2006), A model study of the seasonal mixed layer in the equatorial

- Atlantic, *J. Geophys. Res.*, *111*, C06014, doi:10.1029/2005JC003157.
- Qiao, L., and R. H. Weisberg (1995), Tropical instability wave kinematics: Observations from the tropical instability wave experiment, *J. Geophys. Res.*, *100*, 8677–8693.
- Risien, C. M., and D. B. Chelton (2008), A global climatology of surface wind and wind stress fields from eight years of QuikSCAT scatterometer data, *J. Phys. Oceanogr.*, *38*, 2379–2413, doi: 10.1175/2008JPO3881.1.
- Seo, H., and S.-P. Xie (2011), Response and impact of equatorial ocean dynamics and tropical instability waves in the tropical Atlantic under global warming: A regional coupled downscaling study, *J. Geophys. Res.*, *116*, C03026, doi:10.1029/2010JC006670.
- Seo, H., M. Jochum, R. Murtugudde, A. J. Miller, and J. O. Roads (2007), Feedback of tropical instability-wave-induced atmospheric variability onto the ocean, *J. Climate*, *20*, 5842–5855, doi:10.1175/2007JCLI1700.1.
- Servain, J., J. Picaut, and J. Merle (1982), Evidence of remote forcing in the equatorial Atlantic Ocean, *J. Phys. Oceanogr.*, *12*, 457–463.
- von Schuckmann, K., P. Brandt, and C. Eden (2008), Generation of tropical instability waves in the Atlantic Ocean, *J. Geophys. Res.*, *113*, C08034, doi:10.1029/2007JC004712.
- Weisberg, R. H., and T. J. Weingartner (1988), Instability waves in the equatorial Atlantic ocean, *J. Phys. Oceanogr.*, *18*, 1641–1657.
- Wittenberg, A. T. (2002), ENSO response to altered climate. Ph.D. thesis, Princeton University, 475 pp.
- Wu, Q., and K. P. Bowman (2007a), Multiyear satellite observations of the atmospheric response to Atlantic tropical instability waves, *J. Geophys. Res.*, *112*, D19104, doi:10.1029/2007JD008627.

- 614 Wu, Q., and K. P. Bowman (2007b), Interannual variations of tropical instability waves
615 observed by the Tropical Rainfall Measuring Mission, *Geophys. Res. Lett.*, *34*, L09701,
616 doi:10.1029/2007GL029719.
- 617 Xie, S. P., M. Ishiwatari, H. Hashizume, and K. Takeuchi (1998), Coupled ocean-
618 atmospheric waves on the equatorial front, *Geophys. Res. Lett.*, *25*, 3863–3866,
619 doi:10.1029/1998GL900014.
- 620 Zebiak, S. E. (1993), Air-sea interaction in the equatorial Atlantic region, *J. Clim.*, *27*,
621 1567–1586.

List of Figures

1. Map of a) July 26 - August 2, 2009 AVISO SLA, b) July 26 - August 2, 2009 TMI SST, and c) annual mean TMI SST during 2009. Latitude bands in which TIW variances are computed (black boxes) are shown in a)-b), and the regions where the ATL3 (black box), EUC-nSEC (brown box), and nSEC-NECC (blue box) indices are computed are shown in panel c). Yellow star in a)-b) shows location of 4°N, 23°W PIRATA Northeast Extension mooring.

2. Zonally-averaged (20°W to 0°) standard deviation of the interannual (seasonal cycle removed) a) wind-driven vertical velocity and b) meridional shear of the wind-driven zonal transport terms in equations (2) and (3), respectively, for $r_s^{-1} = 1.5$ day. Colored lines correspond to the first (red), second (green), third (blue), and fourth (magenta) term in those equations, and black lines correspond to the sum of the four terms. Black dashed lines indicate the latitude range of the EUC-nSEC region.

3. Normalized TIW variance in latitude bands along a) 5°N, b) 2°N, c) 0°, d) 2°S, and e) 5°S for the full TMI SST (blue curves) and AVISO SLA (black curves) records. PIRATA horizontal velocity TIW variance (red curve) is overlaid on panel a). Brown lines in a) and b) highlight the years 2006-2009. Seasonal peaks in TIW variance are identified by stars. Correlation between SST and SLA peak TIW variance and significance level of the correlation (assuming independence of annual values) are given in each panel.

4. A comparison of a) ATL3 SST, b) wind stress divergence, and c) wind stress curl indices from 1998 to 2010 (a four-month Bartlett low-pass filter was applied to the indices solely for visualization purposes). Wind stress divergence and curl indices are averaged between 0° and 3°N. Brown lines in a) to c) highlight the years 2006-2009.

Lagged correlations between divergence (solid black curve) and curl (solid blue curve) indices with the ATL3 SST index are shown in panel d). Correlations significant at the 95% level (assuming three independent samples per year) are identified by circles.

5. A comparison of a) ATL3 SST, b) Ekman zonal current shear, and c) total zonal current shear indices from 1998 to 2010 (a four-month Bartlett low-pass filter was applied to the indices solely for visualization purposes). Shear indices are averaged between 3°N and 6°N. Brown lines in a) to c) highlight the years 2006-2009. Lagged correlations between Ekman (solid black curve) and total (solid blue curve) zonal current shear indices with the ATL3 SST index are shown in panel d). Correlations significant at the 95% level (assuming three independent samples per year) are identified by circles.

6. Peak TIW SST variance (blue stars from Figure 3) along 2°N as a function of the five indices: a) June to September ATL3 SST in °C, b) June to September wind stress divergence in $Nm^{-2}(10^3km)^{-1}$, c) May to August wind stress curl in $Nm^{-2}(10^3km)^{-1}$, d) May to August Ekman zonal current shear in $s^{-1} \times 10^{-7}$, and e) May to August total zonal current shear in $s^{-1} \times 10^{-6}$. Correlation and significance level of the correlation (assuming independence of annual values) are given in each panel.

7. Same as Figure 6 except along 5°N.

8. Peak TIW SLA variance (blue stars from Figure 3) along 2°N as a function of the five indices: a) June to September ATL3 SST in °C, b) June to September wind stress divergence in $Nm^{-2}(10^3km)^{-1}$, c) May to August wind stress curl in $Nm^{-2}(10^3km)^{-1}$, d) May to August Ekman zonal current shear in $s^{-1} \times 10^{-7}$, and e) May to August total zonal current shear in $s^{-1} \times 10^{-6}$. Correlation and significance level of the correlation (assuming independence of annual values) are given in each panel.

9. Same as Figure 8 except along 5°N.

10. Correlations between peak TIW a-e) SST and f-j) SLA variance with the five

indices: a, f) ATL3 SST; wind stress b, g) divergence and c, d) curl; as well as d, i)

Ekman and e, j) total zonal current shear. Correlations significant at the 95% (assuming

independence of annual values) are identified by circles.

Table 1. Minimum and maximum TIW variance from 1998 to 2010 and the year of maximum TIW variance along the five latitude bands. Bold values indicate the overall maximum for SST and SLA TIW variance. Note that for the 4°N, 23°W mooring, the minimum and maximum velocity TIW variance are 17.9 and $254.6 \text{ cm}^2\text{s}^{-2}$, respectively, with maximum variance found in 2009.

Latitude	Min σ_{SST}^2 ($^{\circ}\text{C}^2$)	Max σ_{SST}^2 ($^{\circ}\text{C}^2$)	Year Max σ_{SST}^2	Min σ_{SLA}^2 (cm^2)	Min σ_{SLA}^2 (cm^2)	Year Max σ_{SLA}^2
5°N	0.003	0.015	2009	0.095	1.043	2001
2°N	0.004	0.050	2001	0.046	0.251	2010
0°	0.004	0.032	2004	0.048	0.134	1998
2°S	0.001	0.012	2002	0.053	0.241	1998
5°S	0.001	0.013	2005	0.037	0.302	2008

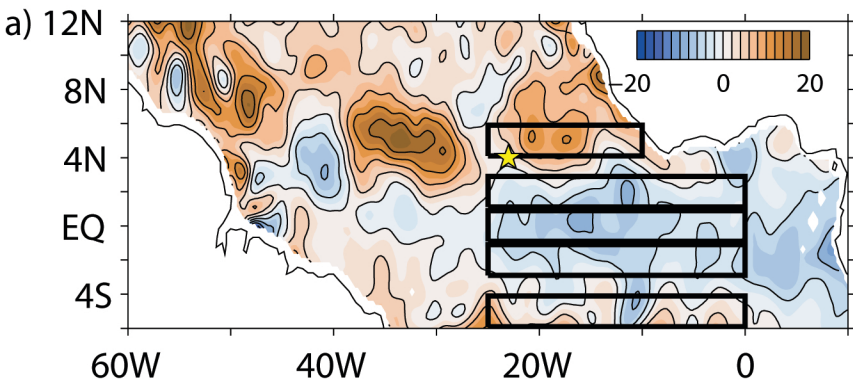
Table 2. Primary and secondary months of SST and SLA peak TIW variance from 1998 to 2010 along the five latitude bands. Percentage of occurrence for the thirteen-year record is listed for each month. If primary month has percentage of occurrence greater than 80%, secondary month is not listed.

Latitude	SST		SLA	
	Month(s)	%	Month(s)	%
5°N	June, July	38, 31	July, June	62, 23
2°N	July, —	85, —	June, July	46, 38
0°	July, August	38, 38	June, July	31, 31
2°S	July, August	69, 23	August, September	46, 46
5°S	July, August	77, 15	July, August	46, 38

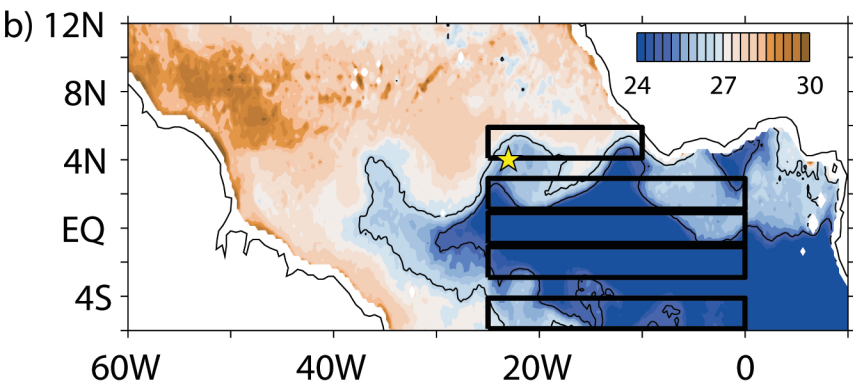
Table 3. Auto- and cross-correlation between SST and SLA seasonal peak TIW variance along the five latitude bands with SST peak variance at 2°N and SLA peak variance at 5°N. Bold values indicates correlations that are at least significant at the 95% confidence level (assuming independence of annual values).

	$\sigma_{SST,2^{\circ}N}^2$	$\sigma_{SLA,5^{\circ}N}^2$		$\sigma_{SST,2^{\circ}N}^2$	$\sigma_{SLA,5^{\circ}N}^2$
$\sigma_{SST,5^{\circ}N}^2$	0.75	0.65	$\sigma_{SLA,5^{\circ}N}^2$	0.58	-
2°N	-	0.58	2°N	0.67	0.60
0°N	0.09	-0.37	0°N	0.12	-0.22
2°S	0.35	0.27	2°S	-0.12	-0.59
5°S	0.56	0.43	5°S	0.39	0.36

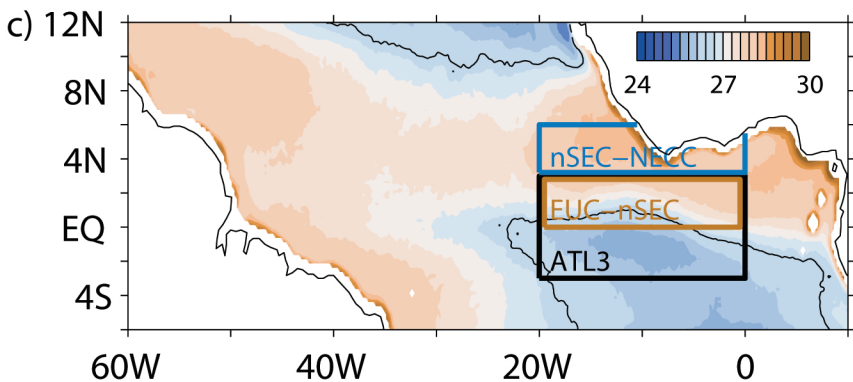
SLA Variance Bands

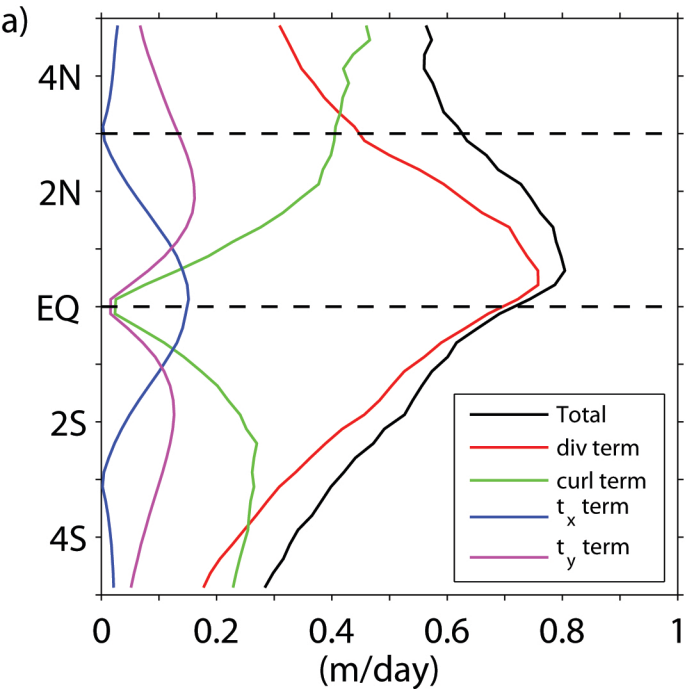
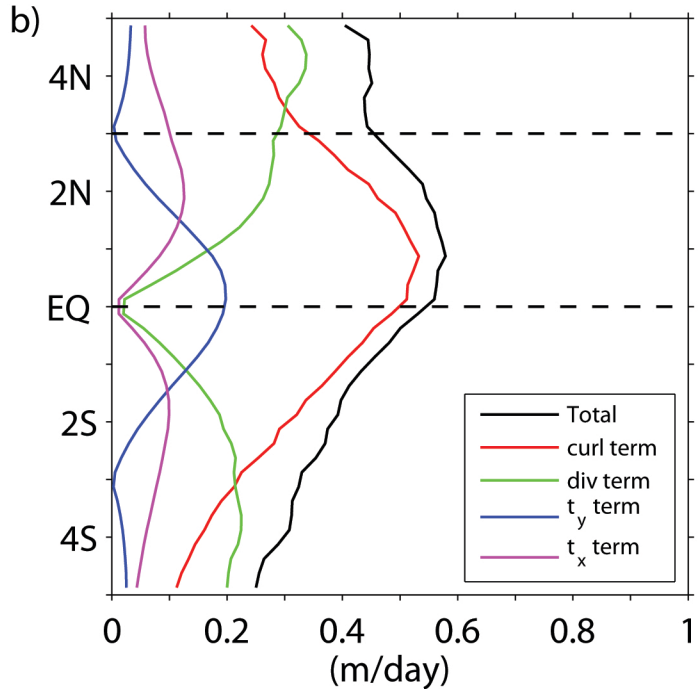


SST Variance Bands

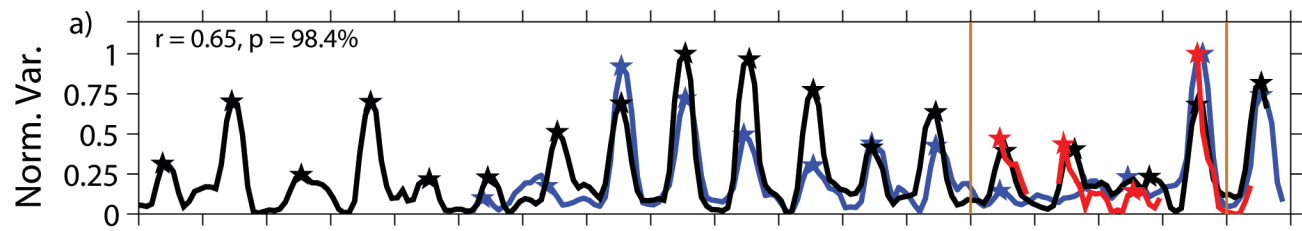


Indices

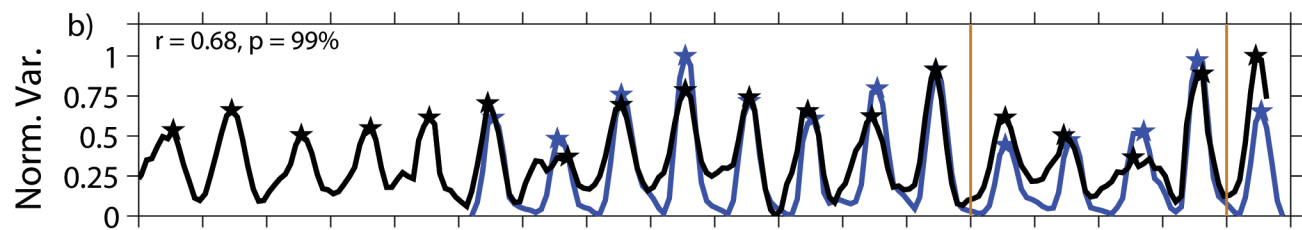


Interannual $s(w_t)$ Interannual $s(dU_t/dy)$ 

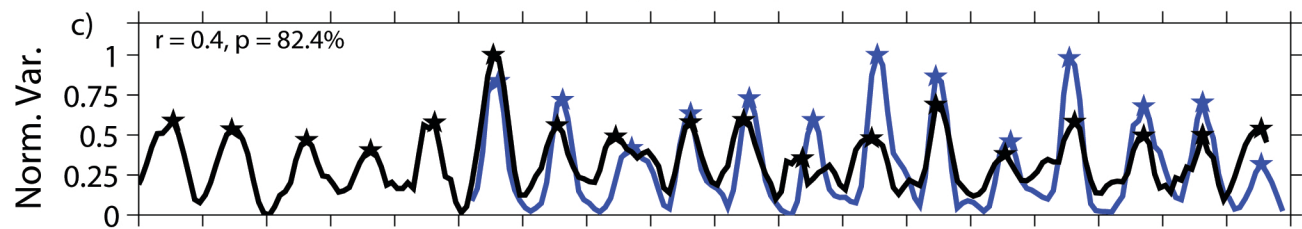
TIW Variance (5N band)



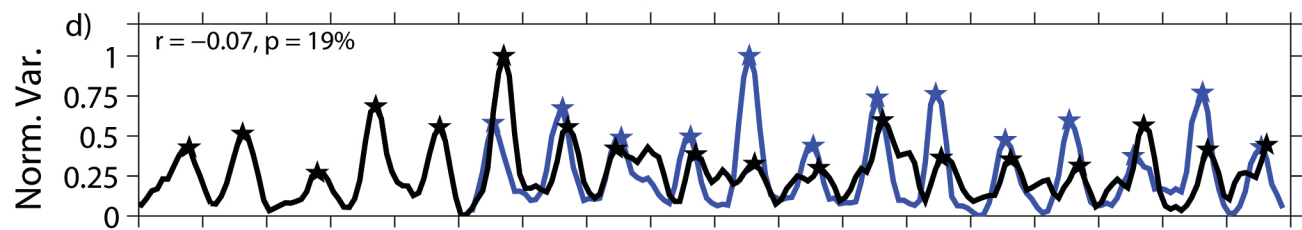
(2N band)



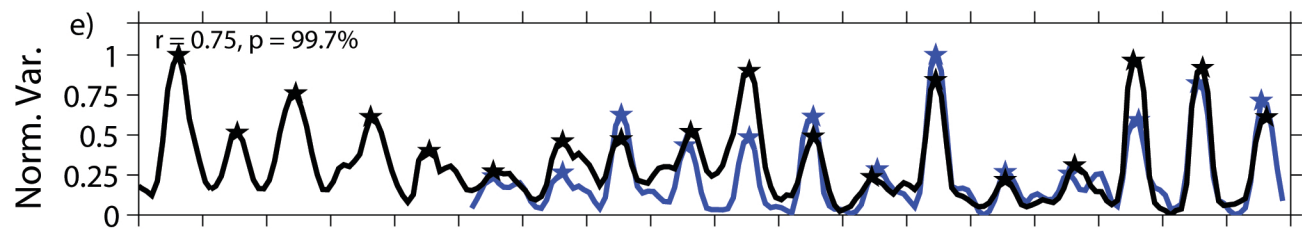
(EQ band)



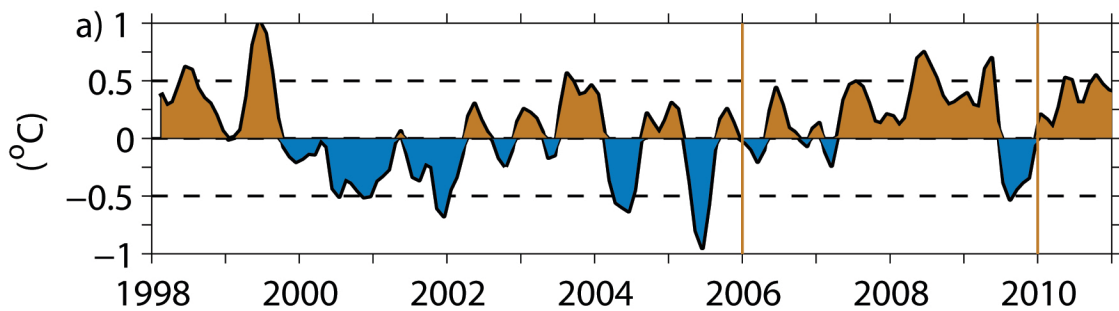
(2S band)



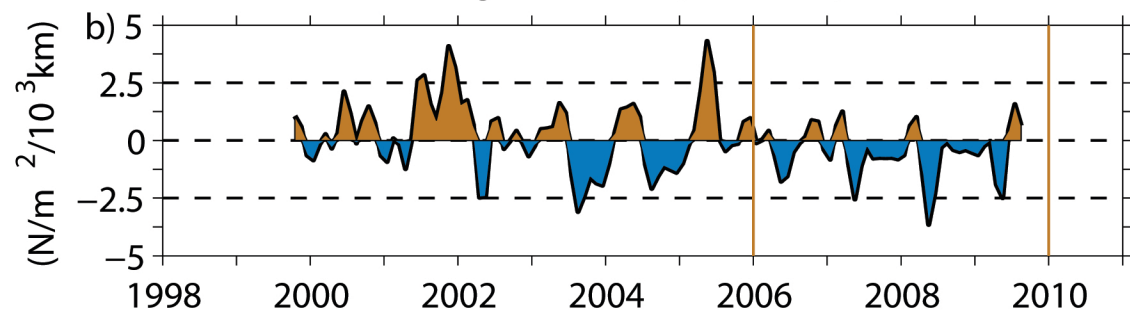
(5S band)



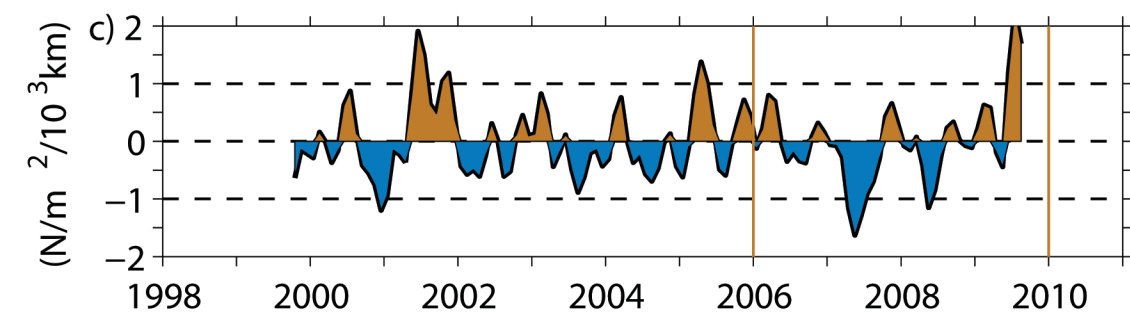
ATL3 index (TMI)



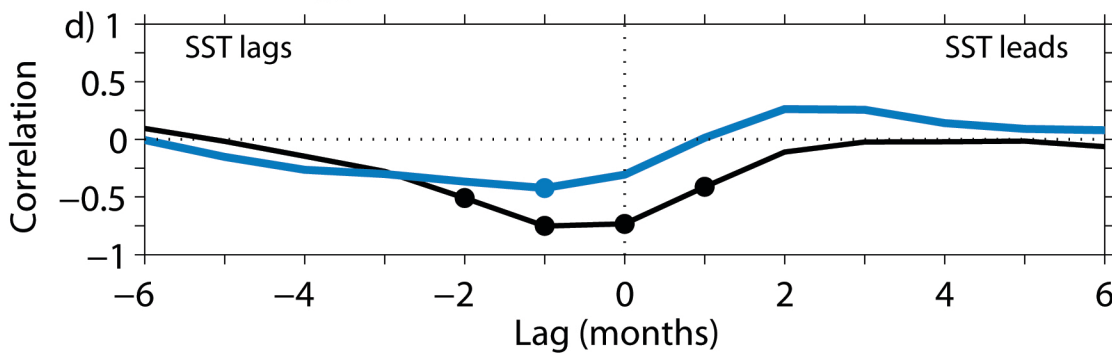
Divergence index (QuikSCAT)



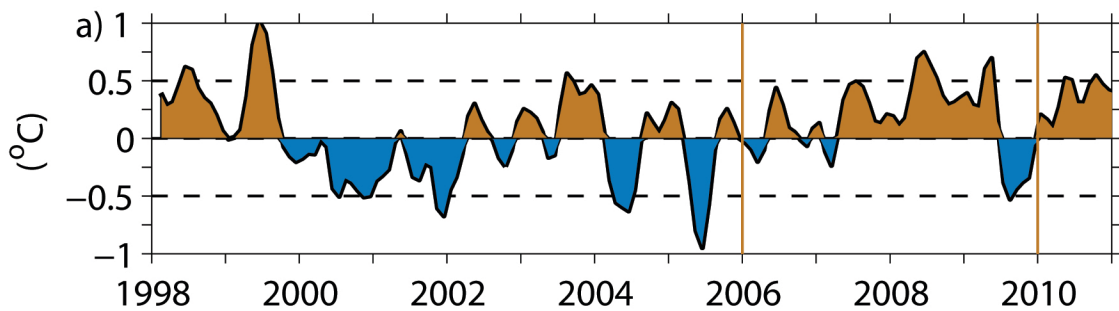
Curl index (QuikSCAT)



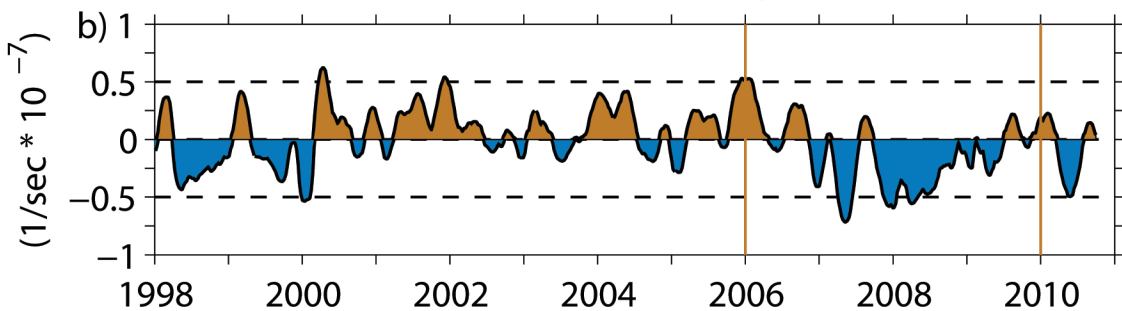
Lagged Correlations with ATL3 SST Index



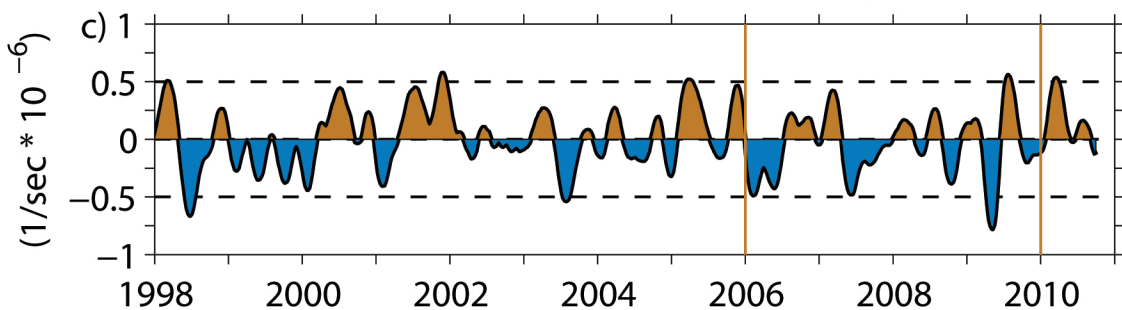
ATL3 index (TMI)



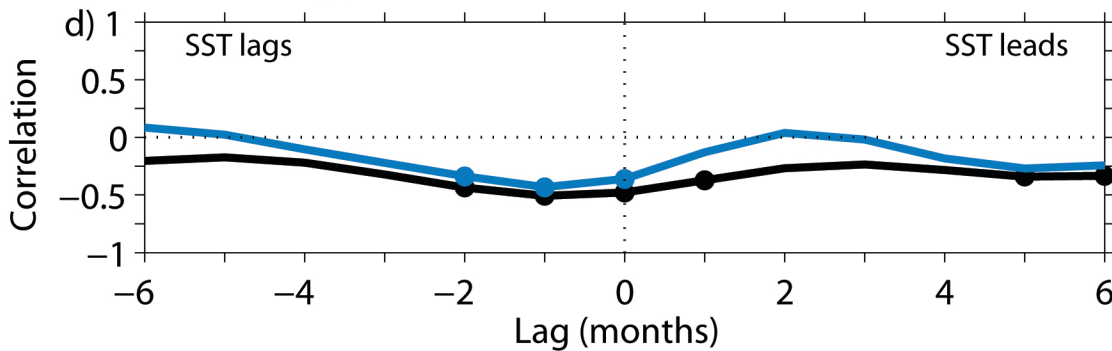
Ekman Shear index (Drifter Synthesis)



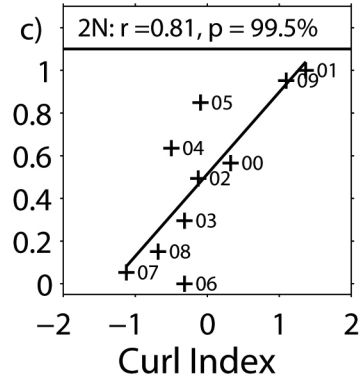
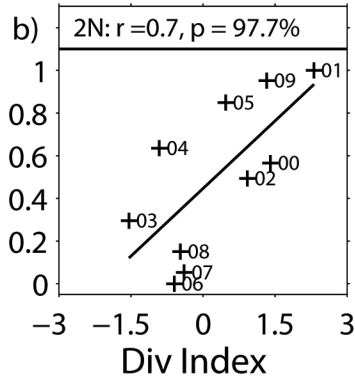
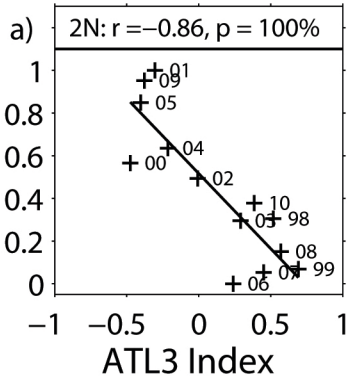
Geostrophic + Ekman Shear index (Drifter Synthesis)



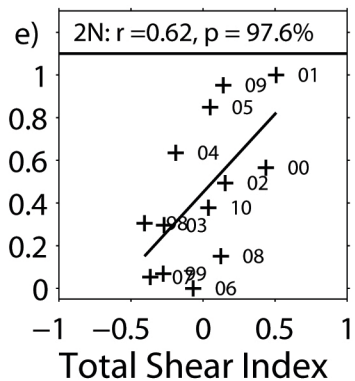
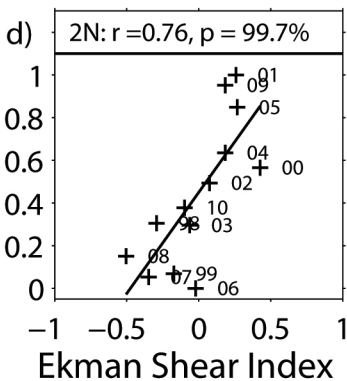
Lagged Correlations with ATL3 SST Index



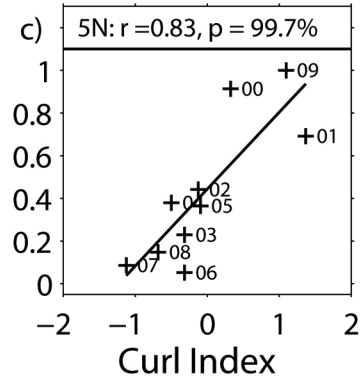
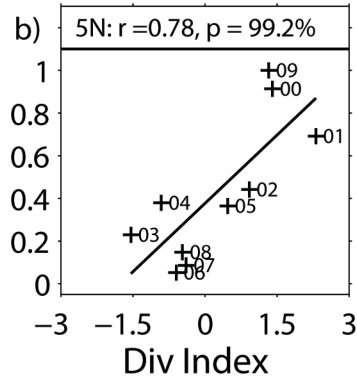
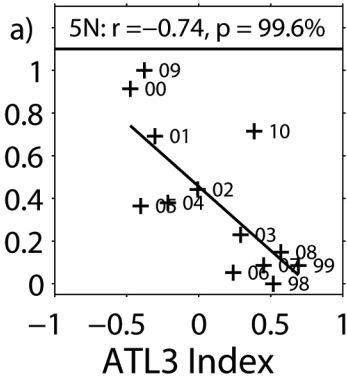
SST Variance



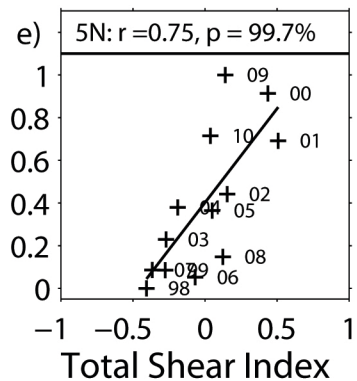
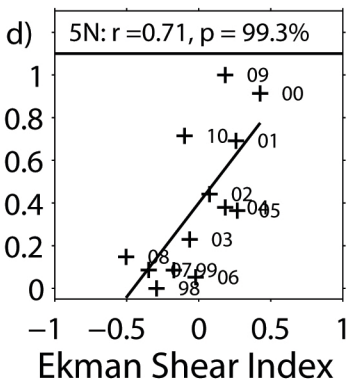
SST Variance



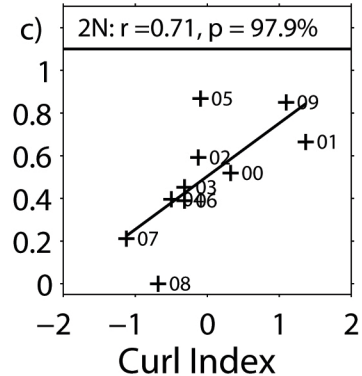
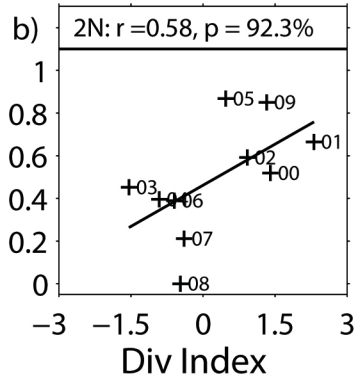
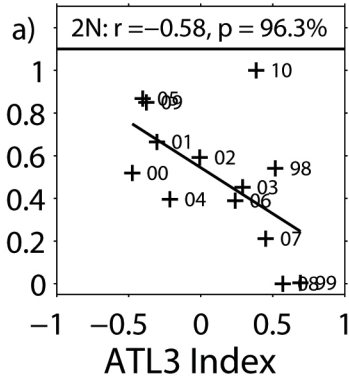
SST Variance



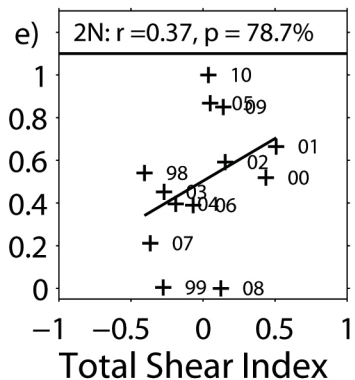
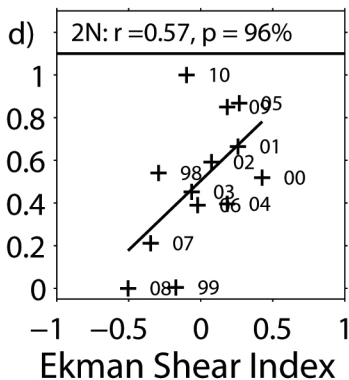
SST Variance



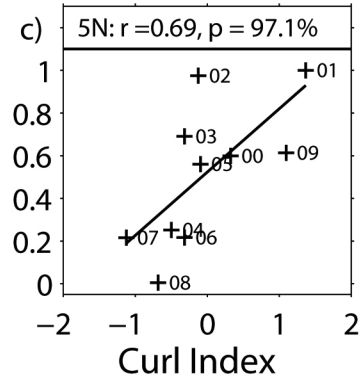
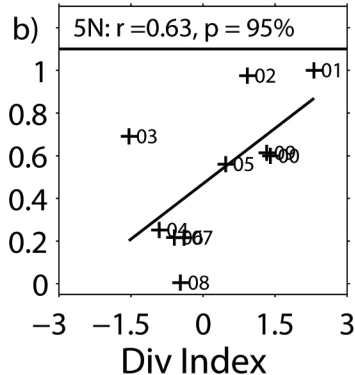
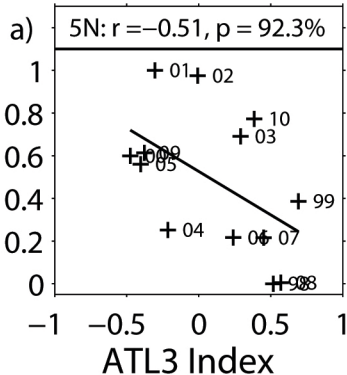
SLA Variance



SLA Variance



SLA Variance



SLA Variance

